RSC Advances

PAPER

View Article Online
View Journal | View Issue

Cite this: *RSC Adv.*, 2017, **7**, 44296

Variation of carbon coatings on the electrochemical performance of $LiFePO_4$ cathodes for lithium ionic batteries†

Weiwei Jiang, Mengqiang Wu,* Fei Liu, Jian Yang and Tingting Feng*

The applications of $LiFePO_4$ (LFP) in high-power lithium ion batteries (LIBs) are limited due to its two major drawbacks: poor electronic conductivity and low lithium ion diffusivity, which could be greatly improved chiefly by reducing the size of LFP crystallites to nanoscale and introducing a conductive carbon-coating layer. In this study, asphalt-derived and glucose-derived carbon proved to be soft carbon-coating (SCC) and hard carbon-coating (HCC), respectively. Asphalt and glucose were therefore used as carbon precursors to prepare varied carbon-coated LFP nanoparticles. The electrochemical properties of the LFP/carbon composites were studied using cyclic voltammetry, electrochemical impedance spectroscopy and charge/discharge cycling. The effects of variation of carbon coatings on the electrochemical performance of $LiFePO_4$ cathodes was investigated in detail, and it was found that LFP/SCC showed a superior performance in capacity and rate capability than that of LFP/HCC. It was therefore concluded that soft carbon coating on LFP exhibits better electrochemical performance than hard carbon coating, demonstrating that asphalt could be used as a cheap and efficient carbon source material of $LiFePO_4$ cathodes for LIBs.

Received 21st July 2017
Accepted 1st September 2017

DOI: 10.1039/c7ra08062j

rsc.li/rsc-advances

1. Introduction

Lithium ion batteries (LIBs) have been increasingly essential in our daily lives due to their wide applications in portable electronic devices, electric vehicles and renewable energy-storage systems.[1] Therefore, advanced LIB technology with high energy and power densities, excellent safety and low cost is urgently required to meet the needs of various applications. As a cathode material for LIB, olivine-structured lithium iron phosphate $LiFePO_4$ (LFP) has become one of the most promising materials with its numerous advantages such as acceptable capacity, outstanding capacity retention, high thermal stability, and environmental friendly nature.[2] However, LFP materials also run up against two major problems of low electric conductivity and poor lithium ion diffusivity, leading to their inadequacy in high-rate applications.[3] Several currently popular approaches have been utilized in an effort to improve the performance of $LiFePO_4$, including reducing the particle size to nanoscale which has been pointed out by John Goodenough *et al.*, to decrease the diffusion path of lithium ions,[2,4] coating of the LFP surface with Cu, Ag or conducting polymers to enhance the electron transport action,[5–7] doping LFP with supervalent cations (*e.g.*, Ga^{3+}, Ti^{4+}, Nb^{5+}) or anions (*e.g.* F^-, Cl^-) to facilitate the lithium ion permeability[8–10] and graphene-modified LFP cathode to enhance the capacity of lithium ion batteries.[11–13] A thin uniform carbon layer could remarkably improve the electronic conductivity of LFP, which therefore has been extensively regarded as an efficient way to enhance the overall battery performance.[2,14] Organic compounds such as glucose,[15] sucrose[16] and citric acid[17] have been proved and widely used as effective and economic carbon sources which could form a homogeneous carbon layer over LFP by *in situ* carbon coating at high temperature. Polymers such as starch,[18] polystyrene[19] and polyaniline[20] have also been under investigation. However, the structure of the carbon coated on the surface of the LFP particles also significantly affects the electrochemical performance of C/LFP.[2,21] Few studies have reported that the high amount of graphitized carbon is more desirable in view of its contribution to the electronic conductivity of the cathode material.[22] Recently, Ren *et al.* successfully investigated that soft contact conductive carbon coated LFP cathode material has better properties than hard carbon coating.[23] As the heat treatment reached the graphitization temperature, the asphalt exhibits a higher degree of graphitization, so asphalt is also known as a precursor of soft carbon,[24] contrary to glucose which is called a hard carbon material.[25]

Herein, we applied asphalt for the carbon encapsulation of LFP. The carbon layer generated by *in situ* carbonization of asphalt could also greatly facilitate encapsulation of the electrochemical performance of LFP cathode material. In this

Center for Advanced Electric Energy Technologies (CAEET), School of Energy Science and Engineering, University of Electronic Science and Technology of China, Chengdu 611731, China. E-mail: mwu@uestc.edu.cn; fengtt@uestc.edu.cn

† Electronic supplementary information (ESI) available. See DOI: 10.1039/c7ra08062j

case, LFP nanosheets were first synthesized by a solvothermal method and subsequently coated with an ultrathin amorphous carbon layer derived from asphalt to form a core–shell architecture. The composite was typically a soft carbon encapsulated LFP (LFP/SCC) due to the formation of a more denser and more uniform carbon layer in the LFP shell, distinguished from the LFP/hard carbon (LFP/HCC) composite derived from glucose. The electrochemical performances of the LFP/HCC and LFP/SCC were examined in the application of LIBs. As anticipated, the LFP/SCC displays a higher electrochemical reactivity and reversibility and therefore delivers superior capacity and better rate performance than LFP/HCC, demonstrating that asphalt could be a facile and efficient carbon source in practical carbon encapsulation process for high-performance LIB cathode material. Obtaining carbon of the same thickness using the inexpensive asphalt as a carbon source in lower amounts is preferred over other commercial carbon sources.

2. Experimental

2.1. Synthesis of $LiFePO_4$

LFP nanosheets were synthesized through a solvothermal method using ethylene glycol (EG) as the solvent. Typically, H_3PO_4 (0.01 mol) was first dissolved in 40 mL of EG solution, and $LiOH \cdot H_2O$ (0.03 mol) was added to the solution with vigorous stirring for 2 h to form a white emulsion, which was then poured into three flasks under inert atmosphere. Subsequently, $FeSO_4 \cdot 7H_2O$ (0.01 mol) and ascorbic acid (0.0032 mol) were added and the resulting solution was stirred until it dissolved completely. The obtained light green mixture was transferred into a 50 mL Teflon lined stainless steel autoclave and heated at 180 °C for 2 h in the oven. Following this, the autoclave was cooled down naturally to room temperature and the reaction products were collected, washed with ethanol and deionized water several times, and then dried at 80 °C in a vacuum oven overnight. The as-synthesized LFP powder was used for subsequent carbon coating using asphalt as the carbon source. To prepare LFP/SCC (20 : 1) composite, 0.025 g of asphalt and 0.5 g of LFP powder were mixed in tetrahydrofuran solvent to form a homogenous slurry, followed by drying in a vacuum oven at 60 °C for 6 h to evaporate the solvent. The mixture was then grinded using an agate mortar, and subjected to calcination in a furnace tube at 700 °C for 6 h under an argon atmosphere. For comparison, LFP/HCC (6 : 1) composite was also prepared using glucose as the carbon source. The carbon coating procedure for LFP/HCC composite was similar to that of LFP/SCC material except that alcohol was used as solvent. It was observed that the carbon content of the carbonized asphalt is more than 95%, while the carbon content of the glucose is only 30–40% after carbonization. In order to make the carbon layers of the two carbon materials the same on carbonization, the mass ratios of LFP and asphalt, as well as LFP and glucose were taken as 20 : 1 and 6 : 1, respectively.

2.2. Material characterizations

The morphologies of the LFP products before and after carbon coating were examined by scanning electron microscopy (SEM, INSPECT F, FEI) at 20 kV. The outer carbon shells and the crystal phases of the LFP nanoparticles were observed by transmission electron microscopy (TEM, FEI Tecnai G2 F20 S-TWIN). X-ray diffraction (XRD, Panalytical Empyrean) was performed at a scanning speed of 5° min^{-1} in the 2θ range from 10° to 80°. The X-ray photoelectron spectroscopy (XPS, Thermo ESCALAB 250XI) was used to analyze the chemical composition and valence state of the elements in the electrode materials. Raman spectra were recorded using a Horiba iHR320 in the 800–2000 cm^{-1} range equipped with an argon laser ($\lambda = 532.05$ nm).

2.3. Electrochemical measurements

In order to investigate the electrochemical properties of the as-synthesized LFP material and its composites, CR2032 coin cells were assembled in an argon-filled glovebox with both moisture and oxygen content below 1 ppm. The cathodes were prepared by mixing 80 wt% of the prepared active materials, 10 wt% of conductive additive (acetylene black) and 10 wt% of poly (vinylidene fluoride) (PVDF) in *N*-methyl pyrrolidinone (NMP). The obtained homogeneous slurry was then spread uniformly on a thin aluminum foil, and dried at 80 °C for 12 h in vacuum before roll pressing. Circular cathodes with a diameter of 15 mm were acquired using a punching machine, and the mass loading of active material was about 1–2 mg cm^{-2}. The cells were assembled with the as-prepared cathode, lithium metal as anode, Celgard 2300 film as separator, 1 M $LiPF_6$ in EC/DEC (1 : 1, v/v) as electrolyte, and were allowed to stand at room temperature for 24 h before testing. The batteries were charged and discharged in the range of 2.5–4.2 V on a LAND CT2001A testing system. Cyclic voltammetry (CV) and electrochemical impedance spectroscopy (EIS) were tested on a CHI 660D electrochemical workstation. CV was carried out between 2.5 and 4.2 V at a scanning rate of 0.5 mV s^{-1}. EIS for the samples was analyzed by applying an amplitude of 5 mV over a frequency range from 100 kHz to 0.01 Hz.

3. Results and discussion

The morphology and particle size of the as-prepared LFP and its core–shell composites are investigated by SEM and TEM. Fig. 1a shows that the LFP synthesized through the solvothermal method consists of uniform nanosheet structure with an average length about 50–100 nm. The SEM images of LFP/SCC and LFP/HCC (Fig. 1d and g) display that both composites retain a nanosphere morphology with a slightly increased diameter after carbon coating, indicating that the LFP nanosheets were homogeneously encapsulated by a carbon shell, and after calcination at high temperature, the structure changes from nanosheet into nanosphere. At the same time, it could be observed that the soft carbon coating is more uniform and compact than the hard carbon coating, and the average particle size is smaller than that of the latter. These characteristics could

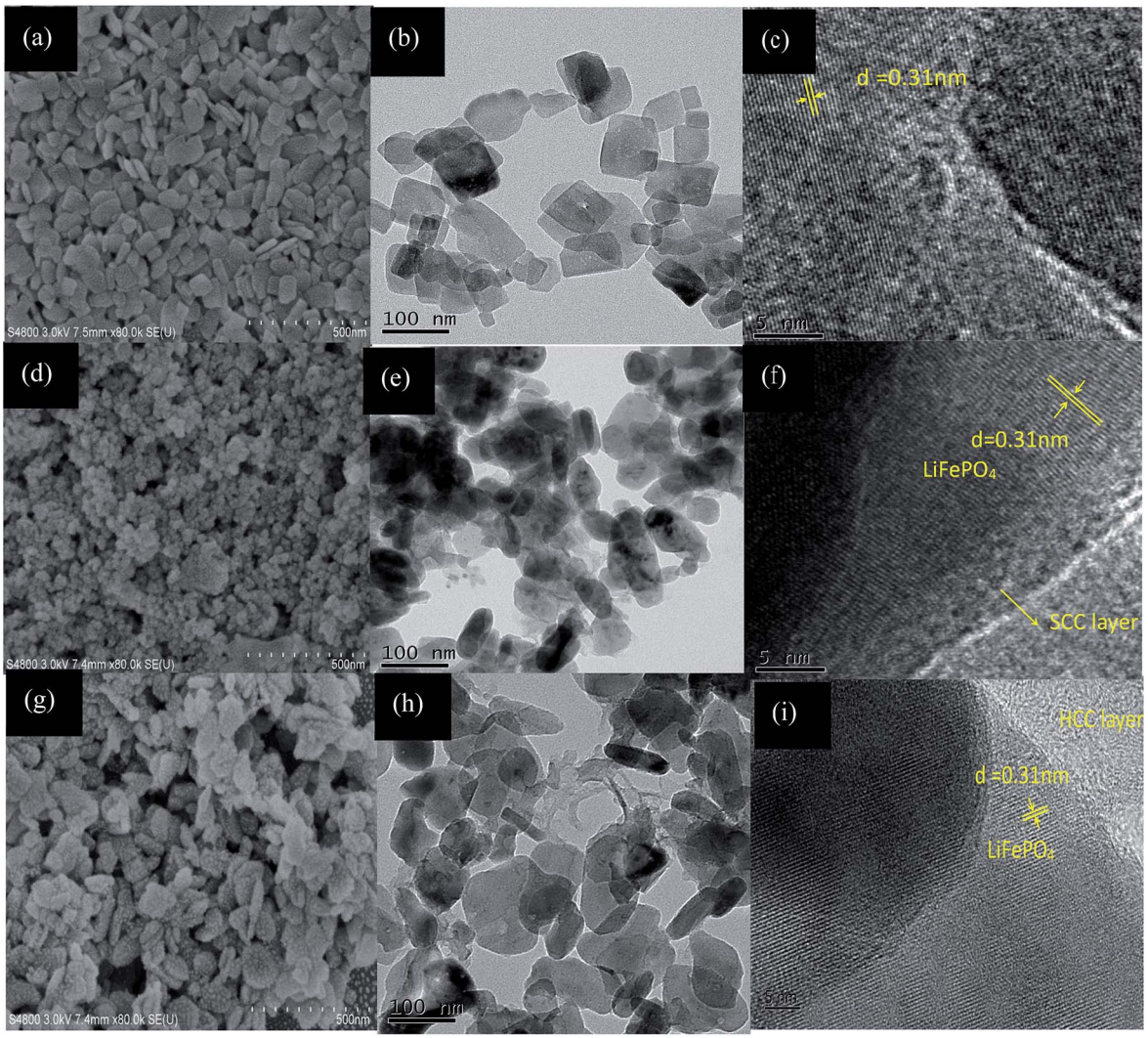

(j)

Element	Weight %	Atomic %	Net Int.	Error %	Kratio	Z	R	A	F
C K	5.82	11.10	45.58	15.48	0.0110	1.1401	0.9245	0.1658	1.0000
O K	42.99	61.53	1497.57	7.59	0.1810	1.0941	0.9476	0.3848	1.0000
P K	19.40	14.34	1676.60	3.92	0.1433	0.9605	1.0058	0.7623	1.0088
FeK	31.79	13.03	1005.90	2.46	0.2805	0.8457	1.0593	1.0053	1.0378

(k)

Element	Weight %	Atomic %	Net Int.	Error %	Kratio	Z	R	A	F
C K	5.80	10.70	53.26	14.67	0.0112	1.1321	0.9289	0.1705	1.0000
O K	46.45	64.39	1898.69	7.39	0.1994	1.0862	0.9517	0.3953	1.0000
P K	18.67	13.37	1859.17	3.83	0.1380	0.9532	1.0093	0.7689	1.0087
FeK	29.08	11.55	1053.83	2.47	0.2551	0.8387	1.0617	1.0063	1.0393

Fig. 1 SEM images of (a) LFP; (d) LFP/SCC; (g) LFP/HCC. The scale bar is 100 nm TEM images of (b) LFP; (e) LFP/SCC; (h) LFP/HCC; HRTEM images of (c) LFP, (f) LFP/SCC and (i) LFP/HCC; EDS of (j) LFP/SCC and (k) LFP/HCC.

also be observed from the TEM diagrams in Fig. 1d and f, which reveal that the LFP/SCC and LFP/HCC nanospheres are coated by a uniform amorphous carbon layer. The high-resolution TEM (HRTEM) results clearly demonstrate that like glucose, asphalt could also provide a uniform and homogenous carbon layer on the surface of the LFP nanosheets, which is beneficial to the

electrochemical performance of LFP. The interplanar spacing of the LFP in the crystallites of LFP, LFP/SCC and LFP/HCC samples is 0.31 nm, corresponding to the (020) plane. Legible lattice fringes prove the good crystalline phase of the sample. Fig. 1j and k are EDS spectra of LFP/SCC and LFP/HCC, respectively. The carbon content of LFP/SCC is 5.8 wt% and that of LFP/HCC is 5.82 wt% based on EDS data. This indicates that the carbonization of asphalt and glucose results in the same thickness of carbon layer on the surface of $LiFePO_4$ cathode material.

The XRD patterns of the LFP, LFP/HCC and LFP/SCC samples are shown in Fig. 2a. The diffraction peaks of the samples that could be observed are well indexed to an orthorhombic olivine structure with the space group *Pnma* (PDF#40-1499-1). The diffraction peaks of the LFP/HCC and LFP/SCC composites are also consistent with that of the LFP sample, indicating minor changes in crystalline phases of the sample after carbon-coating process. However, the intensities of diffraction peaks of LFP/HCC and LFP/SCC composites are greatly increased after carbon-coating treatment particularly in the LFP/SCC sample, indicating that the carbon-coating process could facilitate and improve the crystalline quality of the solvothermal-derived LFP nanosheets probably due to the high-temperature annealing process.

Fig. 2b shows the comparison of the full XPS spectra of the LFP, LFP/HCC and LFP/SCC samples. The full XPS spectrum shown in Fig. 2b shows the binding energy of P 2p, P 2s, and O 1s that were determined to be 133.4, 193.2, and 531.3 eV, respectively. The top-right inset in Fig. 2b shows the high-resolution Fe 2p spectrum in LFP/SCC sample, the binding energies positioned at 711 and 724 eV were ascribed to Fe 2p3/2 and Fe 2p1/2, respectively with an energy separation (ΔE_{Fe}) of 13 eV, which matched well with previously reported results.[26,27] Fig. 2c shows the high resolution XPS spectrum of C 1s of LFP/HCC. Following deconvolution, the C 1s spectrum displayed a lower binding energy featured at 284.5 eV originating from C=C carbon and two higher binding energies featured at 285.6 and 288.5 eV, which were typically assigned to C–O/C–O–C and C=O arising from the residual epoxide, hydroxyl and carboxyl functional groups in glucose.[28] Fig. 2d shows the high

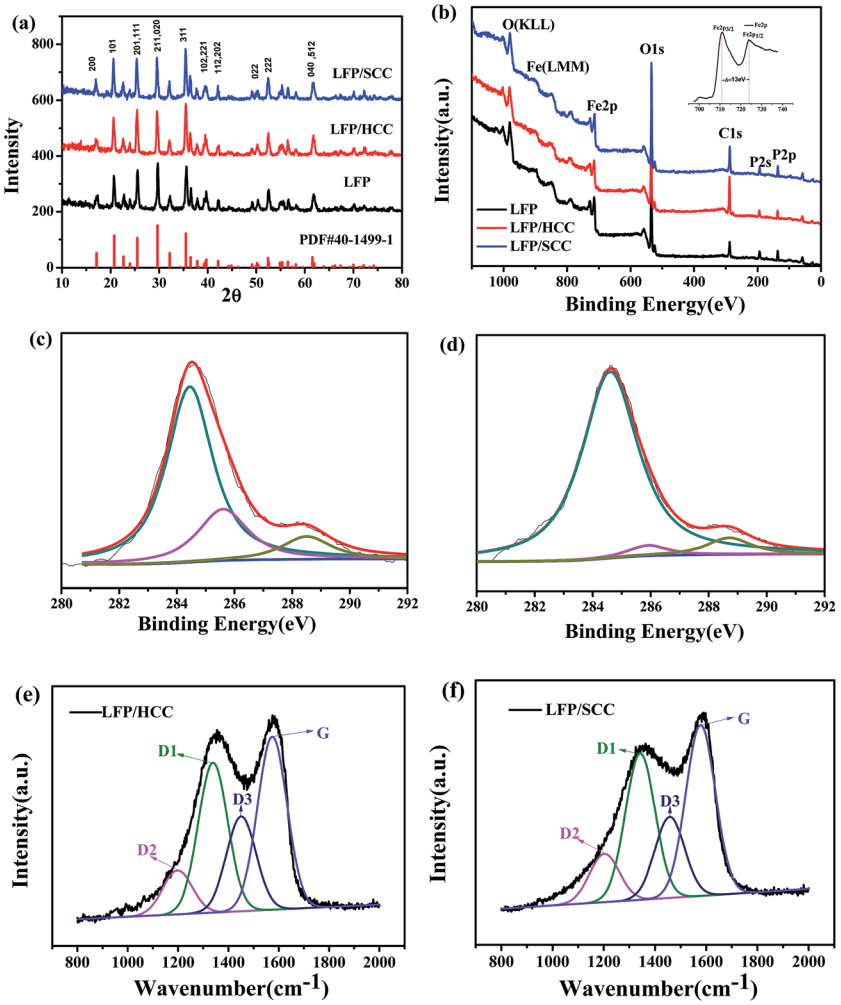

Fig. 2 (a) XRD patterns of LFP, LFP/HCC and LFP/SCC samples; (b) XPS spectra of LFP, LFP/HCC and LFP/SCC samples, the top-right inset shows the high-resolution Fe 2p spectrum; high resolution XPS spectrum of C 1s for (c) LFP/HCC and (d) LFP/SCC samples; Raman spectra of (e) LFP/HCC and (f) LFP/SCC samples.

resolution XPS spectrum of C 1s of LFP/SCC. After deconvolution, the C 1s spectrum displayed the lower binding energy featured at 284.6 eV corresponding to C=C carbon and the higher binding energies featured at 285.9 and 288.7 eV, which were typically assigned to C–O/C–O–C and C=O arising from the residual epoxide, hydroxyl and carboxyl functional groups in asphalt.[29–31] In addition, the smaller L_a value of SCC indicated smaller graphite crystallite size,[23] which is in accordance with the calculated results $L_a = C(\lambda)/(I_{D_1}/I_G)^{-1}$ (ref. 32 and 33) from the integrated intensities of the disorder-induced D_1 and G bands (I_{D_1}/I_G) in Raman spectra (Fig. 2e and f). The extent of graphitized carbon and its ratio to the disordered carbon is usually characterized by the I_{D_1}/I_G (disordered/graphite) ratio in the Raman microprobe spectrum.[21,34] The lower I_{D_1}/I_G ratio is an indication of the higher amount of graphitized carbon. It is well known that the integrated area ratio $A_{(G+D_1)}$ and $A_{(D_2+D_3)}$ in Raman spectrum could also be used to estimate the relative content of the sp^2/sp^3-type carbon.[18,34,35] The larger the area ratio of $A_{(G+D_1)}/A_{(D_2+D_3)}$, the greater the sp^2 carbon content.[23] From the Fig. 2e and f diagrams, it could be observed that the LFP/SCC has a smaller I_{D_1}/I_G (that is, smaller L_a) and a larger area ratio of $A_{(G+D_1)}/A_{(D_2+D_3)}$. This proves that the asphalt-derived carbon has a higher degree of graphitization compared with the glucose-derived carbon.[26] As reported earlier, asphalt is a soft carbon precursor,[24] while glucose is hard carbon precursor.[25] It could be observed from the electrochemical performance diagrams that LFP/SCC is better than LFP/HCC. Therefore, asphalt could be used as an economical and efficient soft carbon coating material.

The electrochemical performances of the LFP/HCC and LFP/SCC materials were evaluated in lithium ion batteries. Fig. 3a shows the charge/discharge profiles for the first two cycles of the LFP/HCC and LFP/SCC batteries, which display charge/discharge capacities of 142.6/139.1 and 162.3/158.3 mA h g^{-1} for the first cycle and 143.2/138.6 and 167/157.2 mA h g^{-1} for the second cycle, respectively. Although a similar coulombic efficiency of 97.5% is obtained for both electrodes, the soft carbon coating gives rise to a higher capacity than the hard carbon coating. Fig. 3b shows the rate performance of the LFP/HCC and LFP/SCC composites. The LFP/HCC electrode presents discharge capacities of 135.6, 134.6, 125, 111.2, 89.9 and 131 mA h g^{-1} at 0.1, 0.2, 0.5, 1, 2 and 0.1C, respectively, showing severe capacity degradation at higher rates due to its inherent drawback of low electronic conductivity. The LFP/SCC electrode delivers 156.3, 159.9, 151.5, 140.1, 120.6 and 153.3 mA h g^{-1} at the corresponding discharge rates. It is worth noting that LFP/

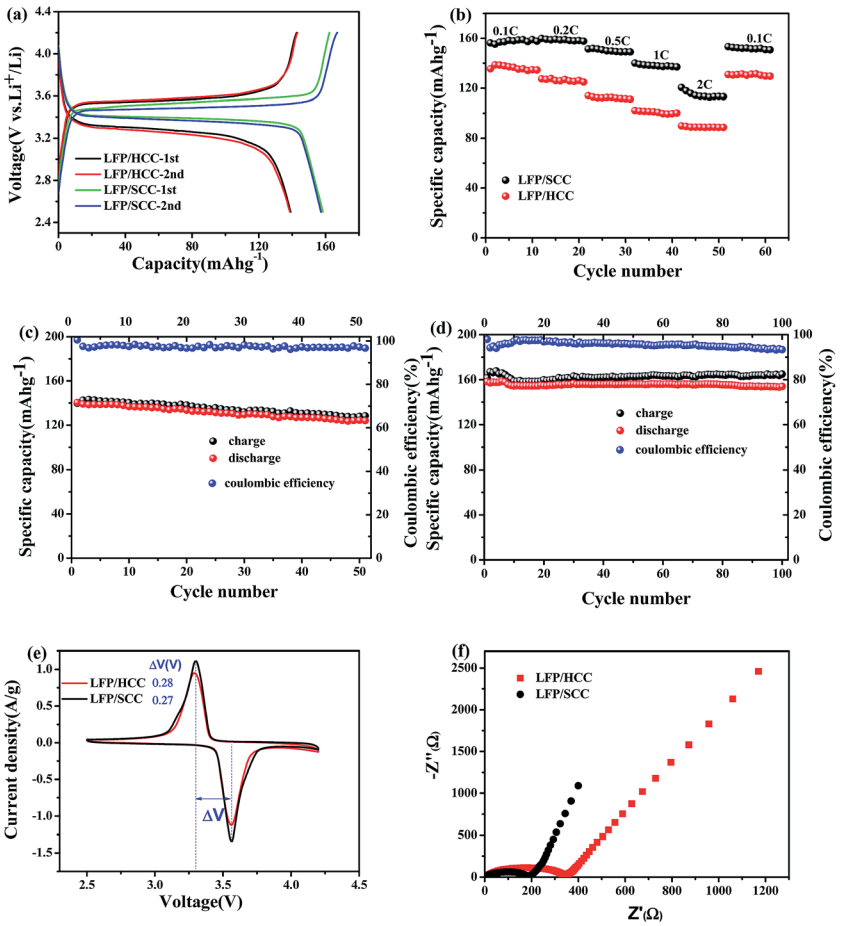

Fig. 3 (a) Charge/discharge in the first two cycles of LFP/HCC and LFP/SCC electrodes; (b) energy capacity of LFP/HCC and LFP/SCC electrodes at 0.1, 0.2, 0.5, 1, 2 and 0.1C; cycle performance of LFP/HCC (c) and LFP/SCC (d) electrodes; (e) CV curves of LFP/HCC and LFP/SCC electrodes; (f) EIS spectra of LFP/HCC and LFP/SCC electrodes.

SCC possesses a superior reversible capacity and rate capability than those of LFP/HCC, especially at a higher rate.

Fig. 3c and d show the cycle performance of the LFP/HCC and LFP/SCC composite electrodes, respectively. The reversible capacity of the LFP/HCC electrode was reduced to 124.1 mA h g^{-1} after 51 cycles at 0.2C, while the capacity of the LFP/SCC electrode was maintained at 154 mA h g^{-1} after 100 cycles at 0.2C, resulting in a capacity retention of 88.3% and 97.3%, respectively. Thus, the soft carbon coating displayed a better cycle performance than hard carbon coating, which could be attributed to the more compact and uniform carbon layers of SCC on the LFP nanosheets.

CV measurements were used to investigate the electrochemical properties of the LFP/HCC and LFP/SCC electrodes and the results are shown in Fig. 3e. It could be observed from the CV profiles that the current density at the redox peaks is enhanced after carbon coating and reaches its highest in LFP/SCC electrodes. Furthermore, the potential difference of the redox peaks, which is relative to the polarization,[36] decreases after carbon coating and attains the least value for LFP/SCC electrodes. All these changes indicate improved electrochemical properties for carbon-coated LFP particularly for LFP/SCC electrode exhibiting a higher electrochemical reactivity and reversibility. Furthermore, the charge/discharge capacity of the electrodes could be partly reflected by the area of the redox peaks, which is associated with the polarization state and the utilization of the active materials. Noticeably, the redox peak area of LFP/SCC sample is a slightly larger than that of LFP/HCC, thus indicating a higher reversible capacity of LFP/SCC. The results of CV analysis are also consistent with that of the galvanostatic charge/discharge measurements, revealing that the LFP/SCC shows optimal electrochemical performance that could be ascribed to the excellent electronic conductivity and better Li ion permeability of the soft carbon coating. EIS spectra were examined to provide a better understanding of the superior battery performance for LFP/SCC. As shown in Fig. 3f, the internal resistance (R_s) of the battery cells is represented by the intercept of the semicircular arc on the horizontal axis in the high frequency region, and the charge transfer resistance (R_{ct}) is the diameter of the semicircle. Noticeably, LFP/SCC electrodes exhibit a decreased R_s value compared with that of LFP/HCC, and the LFP/SCC electrode exhibits a lower R_{ct} value. This indicates that the carbon layer of LFP nanosheets derived from asphalt is more favorable for the transfer of Li ions between the electrode/electrolyte interface.

4. Conclusions

$LiFePO_4$ nanosheets were successfully synthesized through solvothermal method and coated with a soft carbon layer from the *in situ* carbonization of asphalt on calcination. The as-prepared composites exhibited greatly improved electrochemical performances with high reversible capacity, better cycling stability and rate capability at room temperature, which was better than that of the LFP/HCC composites using glucose as the carbon source. The improvements in electrochemical performances are probably ascribed to the soft carbon, which is relatively flat, elastic and easy to deform. In addition, it could form a more uniform and denser carbon layer on the surface of LFP, which helps accelerate the electron transport in $LiFePO_4$ nanosheets and facilitate the diffusion of Li ions between the electrode/electrolyte interfaces during the charge/discharge process. Our study proves that asphalt is an effective carbon source to improve the electrochemical performances of $LiFePO_4$ for high-performance lithium battery applications.

Conflicts of interest

There are no conflicts to declare.

Acknowledgements

The authors are grateful for the financial support from National Natural Science Foundation of China (21503036), Sichuan Science and Technology Support Program (2015GZ0130, 2016000156) and the Fundamental Research Funds for the Central Universities (ZYGX2015KYQD030).

References

1 S. Wang, J. Liao, M. Wu, Z. Xu, F. Gong, C. Chen, Y. Wang and X. Yan, *Part. Part. Syst. Charact.*, 2017, 1700141.
2 T. F. Yi, X. Y. Li, H. Liu, J. Shu, Y. R. Zhu and R. S. Zhu, *Ionics*, 2012, **18**(6), 529–539.
3 Z. Li, D. Zhang and F. Yang, *J. Mater. Sci.*, 2009, **44**(10), 2435–2443.
4 K. Zaghib, A. Mauger, J. Goodenough and C. Julien, Design and Properties of $LiFePO_4$ Nano-materials for High-Power Applications, in *Nanotechnology for Lithium-ion Batteries*, Springer, 2012, pp. 179–220.
5 H. Joachin, T. D. Kaun, K. Zaghib and J. Prakash, *J. Electrochem. Soc.*, 2009, **156**(6), A401–A406.
6 H. C. Dinh, S. I. Mho and I. H. Yeo, *Electroanalysis*, 2011, **23**(9), 2079–2086.
7 F. Croce, A. D. Epifanio, J. Hassoun, A. Deptula, T. Olczac and B. Scrosati, in *A Novel Concept for the Synthesis of an Improved $LiFePO_4$ Lithium Battery Cathode*, 2002.
8 D. Wang, H. Li, S. Shi, X. Huang and L. Chen, *Electrochim. Acta*, 2005, **50**(14), 2955–2958.
9 J. Ma, B. Li, H. Du, C. Xu and F. Kang, *J. Solid State Electrochem.*, 2012, **16**(1), 1–8.
10 L. Yang, L. Jiao, Y. Miao and H. Yuan, *J. Solid State Electrochem.*, 2009, **13**(10), 1541–1544.
11 L. H. Hu, F. Y. Wu, C. T. Lin, A. N. Khlobystov and L. J. Li, *Nat. Commun.*, 2013, **4**(2), 1687.
12 J. Yang, J. Wang, Y. Tang, D. Wang, X. Li, Y. Hu, R. Li, G. Liang, T. K. Sham and X. Sun, *Energy Environ. Sci.*, 2013, **6**(5), 1521–1528.
13 X. Y. Wang, A. Gao, C. C. Lu, X. W. He and X. B. Yin, *Biosens. Bioelectron.*, 2013, **48**, 120.
14 P. M. Pratheeksha, E. H. Mohan, B. V. Sarada, M. Ramakrishna, K. Hembram, P. V. Srinivas, P. J. Daniel, T. N. Rao and S. Anandan, *Phys. Chem. Chem. Phys.*, 2016, **19**(1), 175.

15 Z.-R. Chang, H.-J. Lv, H.-W. Tang, H.-J. Li, X.-Z. Yuan and H. Wang, *Electrochim. Acta*, 2009, **54**(20), 4595–4599.
16 J.-K. Kim, G. Cheruvally and J.-H. Ahn, *J. Solid State Electrochem.*, 2008, **12**(7–8), 799–805.
17 M. Gaberscek, R. Dominko, M. Bele, M. Remskar and J. Jamnik, *Solid State Ionics*, 2006, **177**(35), 3015–3022.
18 S. H. Luo, Z. L. Tang, J. B. Lu and Z. T. Zhang, *Chin. Chem. Lett.*, 2007, **18**(2), 237–240.
19 Y. Zhou, C. Gu, J. Zhou, L. Cheng, W. Liu, Y. Qiao, X. Wang and J. Tu, *Electrochim. Acta*, 2011, **56**(14), 5054–5059.
20 Y. Wang, Y. Wang, E. Hosono, K. Wang and H. Zhou, *Angew. Chem., Int. Ed.*, 2008, **47**(39), 7461–7465.
21 Y. Hu, M. M. Doeff, R. Kostecki and R. Finones, *J. Electrochem. Soc.*, 2003, **151**(8), A1279–A1285.
22 H. C. Shin, W. I. Cho and H. Jang, *Electrochim. Acta*, 2006, **52**(4), 1472–1476.
23 W. Ren, K. Wang, J. Yang, R. Tan, J. Hu, H. Guo, Y. Duan, J. Zheng, Y. Lin and F. Pan, *J. Power Sources*, 2016, **331**, 232–239.
24 Y. Zhai, Y. Dou, D. Zhao, P. F. Fulvio, R. T. Mayes and S. Dai, *Adv. Mater.*, 2011, **23**(42), 4828–4850.
25 Y. Bai, Z. Wang, C. Wu, R. Xu, F. Wu, Y. Liu, H. Li, Y. Li, J. Lu and K. Amine, *ACS Appl. Mater. Interfaces*, 2015, **7**(9), 5598–5604.
26 F. Yu, J.-J. Zhang, Y.-F. Yang and G.-Z. Song, *J. Mater. Chem.*, 2009, **19**(48), 9121–9125.
27 H. Yang, X.-L. Wu, M.-H. Cao and Y.-G. Guo, *J. Phys. Chem. C*, 2009, **113**(8), 3345–3351.
28 B. Wang, T. Liu, A. Liu, G. Liu, L. Wang, T. Gao, D. Wang and X. S. Zhao, *Adv. Energy Mater.*, 2016, **6**(16), 1600426.
29 P.-X. Hou, C. Liu and H.-M. Cheng, *Carbon*, 2008, **46**(15), 2003–2025.
30 Y. Song, X. Wang, C. Zhao, K. Qu, J. Ren and X. Qu, *Chemistry*, 2010, **16**(12), 3617–3621.
31 A. E. Goode, N. D. Hine, S. Chen, S. D. Bergin, M. S. Shaffer, M. P. Ryan, P. D. Haynes, A. E. Porter and D. W. Mccomb, *Chem. Commun.*, 2014, **50**(51), 6744–6747.
32 M. Pawlyta, J. N. Rouzaud and S. Duber, *Carbon*, 2015, **84**, 479–490.
33 L. Cancado, K. Takai, T. Enoki, M. Endo, Y. Kim, H. Mizusaki, A. Jorio, L. Coelho, R. Magalhaes-Paniago and M. Pimenta, *Appl. Phys. Lett.*, 2006, **88**(16), 163106.
34 J. D. Wilcox, M. M. Doeff, M. Marcinek and R. Kostecki, *J. Electrochem. Soc.*, 2006, **154**(5), A389.
35 M. Maccario, L. Croguennec, B. Desbat, M. Couzi, F. Le Cras and L. Servant, *J. Electrochem. Soc.*, 2008, **155**(12), A879–A886.
36 J. Yang, M. Wu, F. Gong, T. Feng, C. Chen and J. Liao, *RSC Adv.*, 2017, **7**(39), 24418–24424.